CHAPTER IV
RESULTS AND DISCUSSION

4.1 Characterizations of eggshell, calcium oxide (CaO) and hydroxyapatite (HAp)

FT-IR spectra of raw material eggshell, CaO synthesized from eggshell by thermal treatment at 900 °C for 1 h, and HAp prepared from CaO via sol-gel process are shown in Fig.4.1. As expected, the eggshell spectrum in Fig.4.1 (a) indicates chemical functional groups of both organic and inorganic matters. The peak around 3000–2500 cm^{-1} corresponded to –C-H stretching while the broad peak at approximately 3428 cm^{-1} attributed to –OH stretching from residual water and –NH stretching of protein containing in the eggshell. The main inorganic composition in the eggshell is calcium carbonate ($CaCO_3$), giving three important peaks at 1450, 873, and 700 cm^{-1} which are characteristics of the C–O asymmetric stretching, out-of plane, and in-plane bending modes, respectively. (Engin *et al.*, 2006)

After the eggshell was heated under air at 900 °C for 1 h, the organic part was combusted into carbon dioxide (CO_2) whereas the inorganic matter, $CaCO_3$, was converted to CaO, and also CO_2, as shown in the equation (1).

$$CaCO_3 \xrightarrow{\Delta} CaO + CO_2 \qquad (1)$$

The FT-IR spectrum of the obtained CaO is shown in Fig. 1 (b). As can be seen, the combustion of the eggshell resulted in no peaks at 3000–2500 cm^{-1}, belonging to organic matter, indicating complete degradation of the organic part. The peak at 3640 cm^{-1} was belong to -OH of calcium hydroxide ($Ca(OH)_2$) resulted from the reaction of CaO and water in the air. (Saito *et al.*, 2008) In addition, the presence of the peaks at 1450 and 873 cm^{-1} indicating the carbonate group was still existed although the intensity of this peak decreased.

Hydroxyapatite synthesized from CaO and orthophosphoric acid via sol-gel process follows the reactions shown in the equations (2)-(4). (Sanosh *et al.*, 2009)

$$CaO + 2HNO_3 \longrightarrow Ca(NO_3)_2 + H_2O \quad (2)$$

$$H_3PO_4 + 3NH_4OH \longrightarrow (NH_4)_3PO_4 + 3H_2O \quad (3)$$

$$6(NH_4)_3PO_4 + 10Ca(NO_3)_2 + 2NH_4OH \longrightarrow Ca_{10}(PO_4)_6(OH)_2 + 20NH_4NO_3 \quad (4)$$

The FT-IR spectrum of the synthesized HAp is given in Fig.1(c). Two important chemical functional groups, indicating the HAp, were phosphates (PO_4^{3-}) at 1050, 1020, 961, 572, and 470 cm^{-1} and hydroxyl group (-OH) at 3571 and 634 cm^{-1}. (Sanosh *et al.*, 2009)

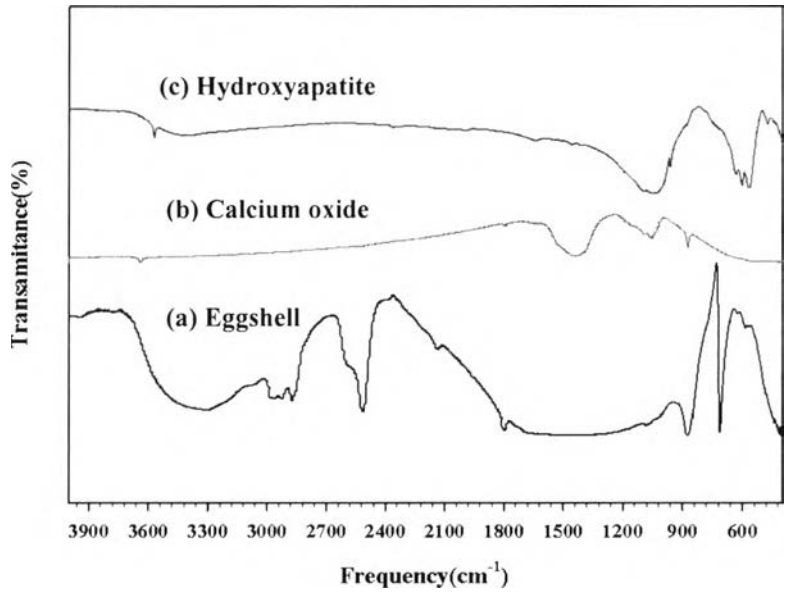

Figure 4.1 FT-IR spectra of (a) eggshell, (b) CaO, and (c) HAp.

X-ray diffraction was an important tool to inform phase composition, average crystalline size, and fraction of crystalline phase. Figure 4.2 (a) shows the XRD pattern of the eggshell, giving the peaks at 2θ (h k l) = 23.02° {012}, 29.35° {104}, 36.06° {110}, 39.48° {113}, 43.30° {202}, 47.36° {024}, 48.65° {116}, 57.55° {122}, 61.34° {119}, 62.72° {125}, 64.67° {300}, 69.58° {217}, 72.67° {218}, and 76.80° {200}, corresponding to the peaks of $CaCO_3$, in agreement with those appeared in JCPDS 5-0586. Figure 4.2 (b) is the calcined eggshell at 900 °C for 1 h, referring to CaO (JCPDS 37-1497) and consisting of 2θ {h k l} = 32.26° {111},

37.40° {200}, 53.82° {220}, 64.22° {311} and 67.44° {222}. It is worth noting that the XRD pattern of the calcined sample also contained crystalline phase of $CaCO_3$, but its intensity decreased, as compared to the eggshell pattern. Figure 4.2 (c) indicates the XRD pattern of the synthesized HAp, giving a hexagonal crystal structure with the main peaks at 2θ {h k l} = 26.0° {002}, 29.06° {210}, 31.8° {211}, 32.24° {112}, 32.98° {300}, 34.14° {202}, 39.90° {310}, 46.96° {222}, 49.60° {213}, 50.20° {321} and 53.28° {004} similar to the standard HAp (JCPDS 9-432). From the data of these peaks, average crystalline size of HAp and the fraction of crystalline phase were calculated using the Scherrer equation, as shown in equations 5 and 6, respectively. (Siva Rama Krishna *et al.*, 2007)

$$D = \frac{K\lambda}{\beta\cos\theta} \qquad (5)$$

$$D = 0.5^{*} \cos(26)$$

$$D = 3.0852 \text{ Å} = 30.852 \text{ nm}$$

D is the average crystallite size (Å); K is the shape factor (K = 0.9)

λ is the wavelength of the X-rays (k = 1.54056 Å for Cu Kα radiation)

β is the full width at half maximum at crystalline plane of {211}

θ is is the Bragg's diffraction angle at the {211} crystalline plane

$$X_c = 1 - \frac{V_{112/300}}{I_{300}} \qquad (6)$$

$$X_c = 1 - \frac{7.12}{15.697} = 0.453589$$

X_c is the fraction of crystalline phase

I_{300} is the intensity of {300} diffraction peak

$V_{112/300}$ is the intensity of the hollow between {112} and {300} diffraction peaks of HAp.

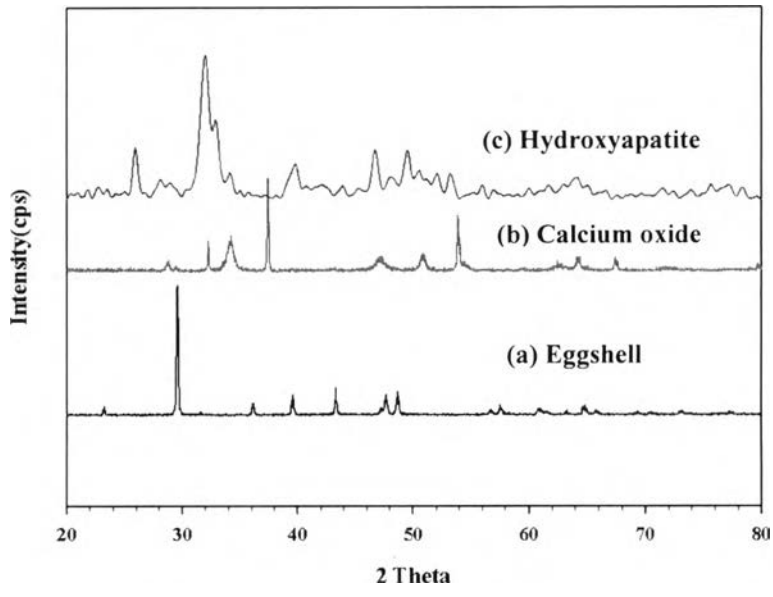

Figure 4.2 XRD patterns of (a) eggshell, (b) CaO, and (c) HAp.

Figure 4.3 presents the thermal properties of the samples obtained in this study. Figure 4.3(a) is belonging to the eggshell, showing two steps of the weight loss. The first weight loss, approximately 5 %, at 270°–400 °C indicated decomposition of organic matter and the other weight loss, 42.2 %, at 450° to 750 °C corresponded to the phase formation of $CaCO_3$ transforming to CaO by freeing CO_2, as explained in equation (1). The percentage of ceramic yield of eggshell is 52.8%. Both CaO and HAp (Fig. 3 (b) and (c), respectively) gave constant weight at higher 500 °C, indicating their thermal stability. TGA thermogram of CaO gave about 6% weight loss between 375° and 400 °C, attributing to decomposition of $CaCO_3$ residue into CaO, while that of HAp (Fig. 3(c)) appeared no weight loss throughout the analysis, indicating that the synthesized HAp has a good thermal stability for the whole temperature range. (Eric *et al.*, 2007)

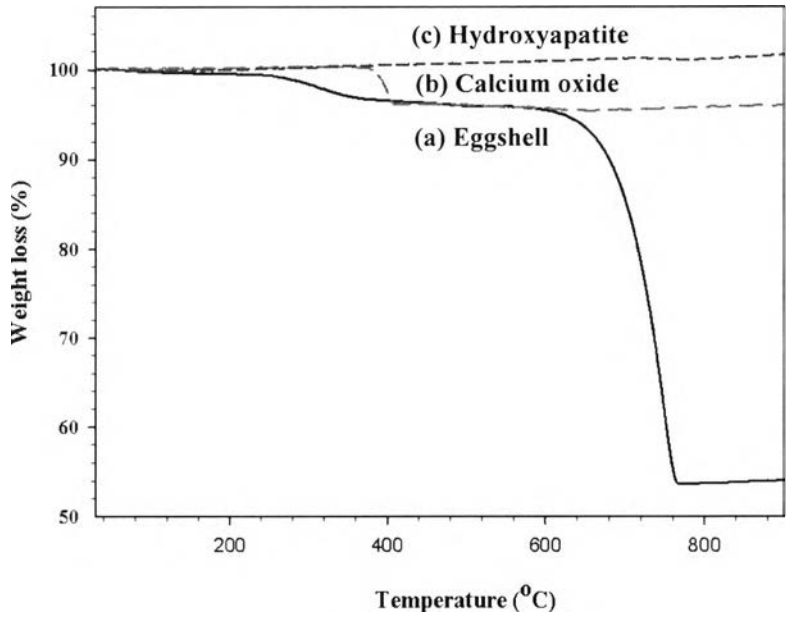

Figure 4.3 TGA thermograms of (a) eggshell, (b) CaO, and (c) HAp.

The morphologies of the samples are shown in Fig. 4.4, 4.5, and 4.6. Figure 4.4 is obtained from ground and sieved eggshell having particle size less than 180 micron, as also indicated in the SEM micrographs.

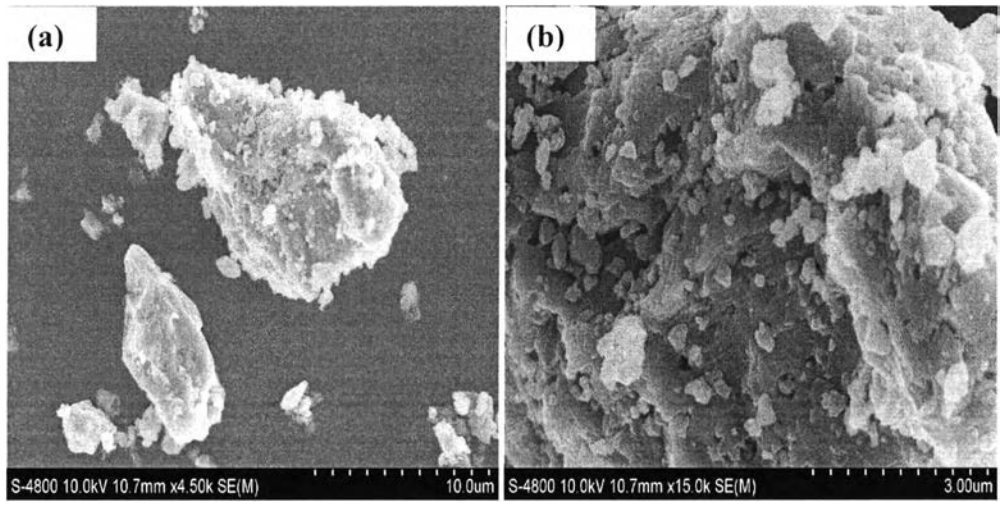

Figure 4.4 SEM micrographs of eggshell with (a) low and (b) high magnifications.

Figure 4.5 (a-b) is the SEM images of CaO resulted from calcinations of the eggshell. The obtained CaO had spherical shape and smaller size (4–10 micron) than the eggshell particles due to the removal of the organic part in the eggshell.

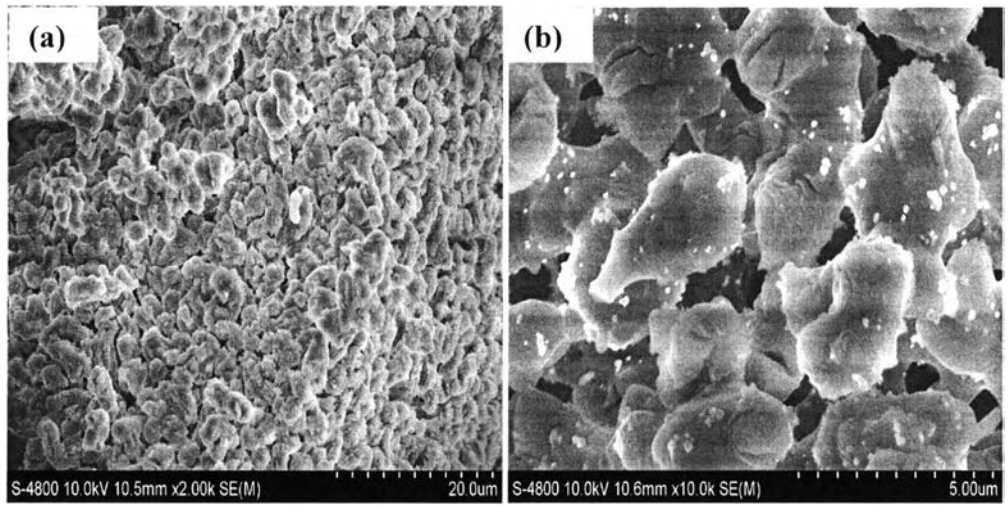

Figure 4.5 SEM micrographs of CaO with (a) low and (b) high magnifications.

The SEM micrographs of the HAp are shown in Fig. 4.6 (a-b), giving irregular shape and also agglomerated particles.

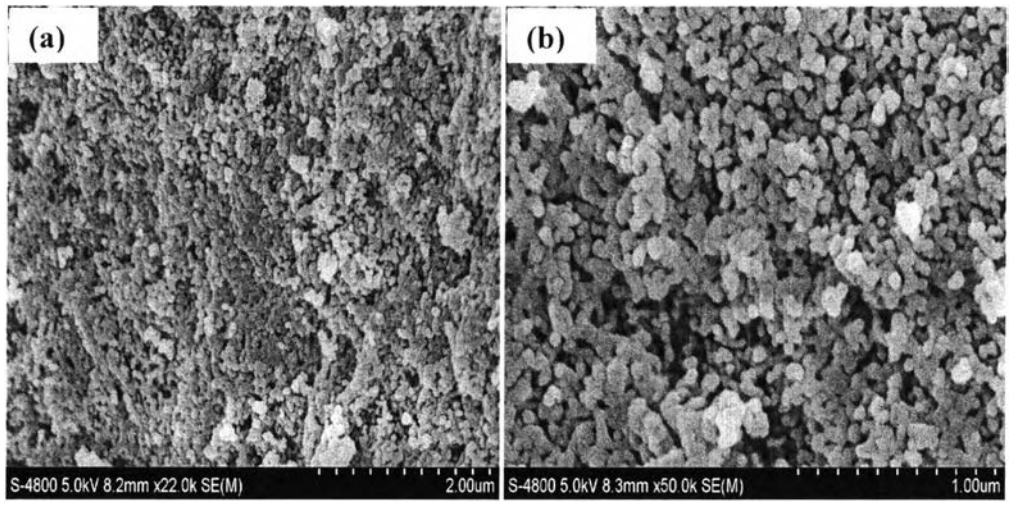

Figure 4.6 SEM micrographs of HAp with (a) low and (b) high magnifications.

The result of agglomerated HAp can be explained using the nucleation–aggregation–agglomeration–growth mechanism, as described by Rodriguez-Clemente *et al.*, shown in Fig. 4.7. There are three steps of the mechanism for agglomerated particles of HAp. The first step is the nucleation and growth to form nanocrystalline of HAp, followed by aggregation and agglomeration of the particles in nanometer size by physical attraction which occur surface free energy minimization of particle. The last step is the crystal growth at constant residual supersaturation. (Sanosh *et al.*, 2009 and Rodríguez *et al.*, 1998)

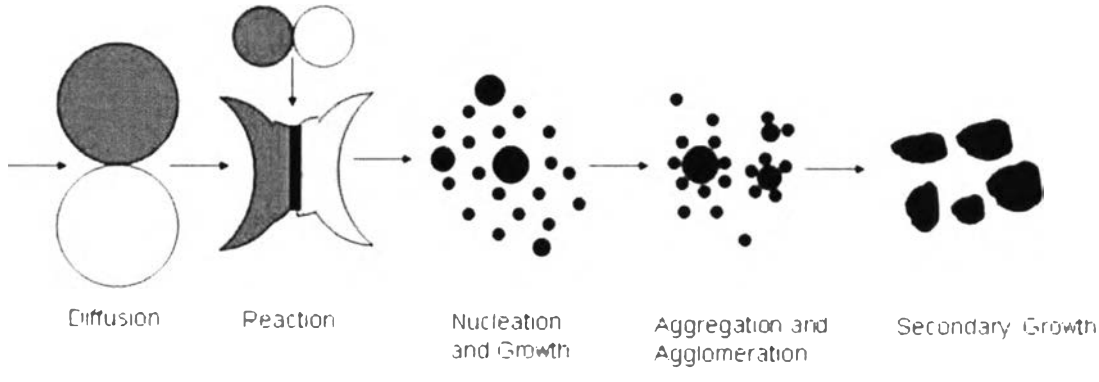

Figure 4.7 Schematic representation of the nucleation and growth mechanism of HAp. (Randolph and Larson *et al.*, 1986 and Rodríguez *et al.*, 1998)

4.2 Characterizations of CaO/HAp - polyvinyl alcohol (PVA) hybrid aerogel

Volumetric shrinkage of the sample can be calculated, using the following equation;

$$\%\text{Shrinkage} = \frac{V_{wet} - V_{dry}}{V_{wet}} \times 100 \qquad (7)$$

V_{wet}= Volume of wet sample which is not eliminated water.

V_{dry} = Volume of dried sample which is completely eliminated water.

The volumetric shrinkage of areogel material is an important factor for the fabrication via freeze dry method and affects on the physical and mechanical properties of the materials. Figure 4.8 represents percent shrinkage of the aerogel

material obtained from various ratios of PVA and CaO and percent weight of PVA in water. It was found that an increase of the PVA content led to an increase in the volume shrinkage of the aerogel material because PVA has high molecular weight and flexible chain, and when the solvent in the aerogel material was eliminated via freeze dryer, the chains of PVA in the resulting material were shrunk. Therefore, the higher ratios of PVA resulted in the more volume shrinkage because of the more PVA chains. From Fig. 4.8, it can be estimated that the optimum ratio of PVA and CaO is 20:80. When considering the percent weight of PVA in water, it was found that the lower percentage of PVA in water gave the higher shrinkage because it has more space area after removing water from the material. However, 5% PVA in water showed higher shrinkage than 4.5% PVA because the 5% percent PVA provides the more viscous, which affects difficulty of dispersion and distribution of CaO in PVA solution. (Safronova *et al.*, 2007 and Krokida *et al.*, 1998)

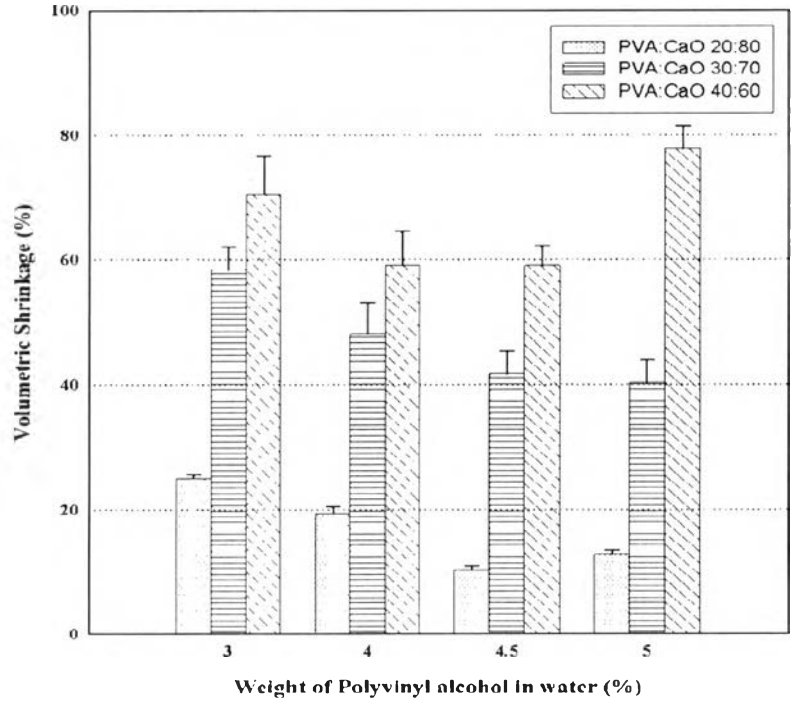

Figure 4.8 Percentage of shrinkage using various ratios of PVA and CaO and different percentages of PVA in water.

In this work, two types of calcium compound are studied to compare, CaO and HAp, which are biomaterial for bone application. Calcium oxide is a bioresorbable biomaterial which can be dissolved and replaced by bone tissue, but HAp is a bioactive biomaterial, having chemical composition like-bone and capable to form chemical bonding with the host bone. Therefore, it is interesting to study the effect of both calcium compounds on the physical and the mechanical properties of areogel material by fixing the optimum of PVA and calcium compound at 20:80. The volume shrinkage of the aerogel material using both calcium compound types and percent weight of PVA in water showed the results in Fig. 4.9. As can be seen, PVA-HAp areogel has lower volume shrinkage than PVA-CaO because PVA chemically interacts with HAp, as shown in Fig. 4.10, thus resulting in good compatibility, dispersion, and distribution. (Safronova *et al.*, 2007)

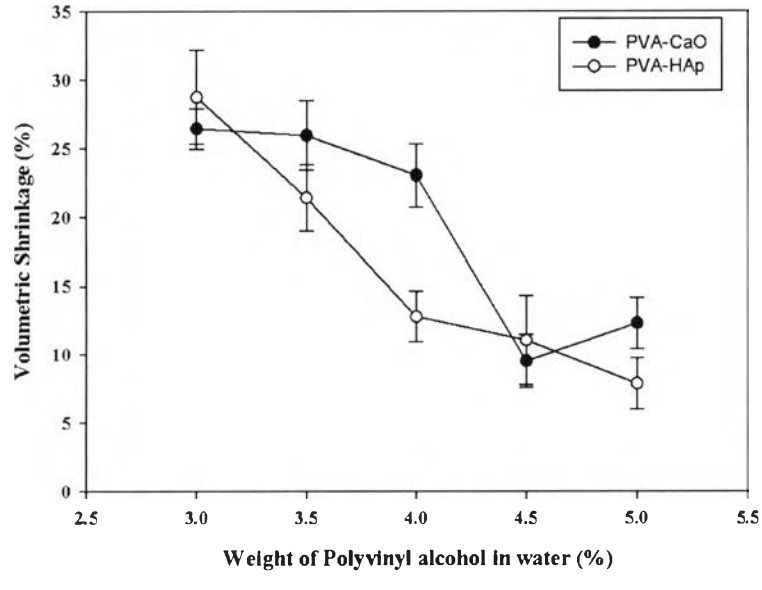

Figure 4.9 Percentage of shrinkage of CaO/HAp - PVA hybrid aerogel using different percentages of PVA in water.

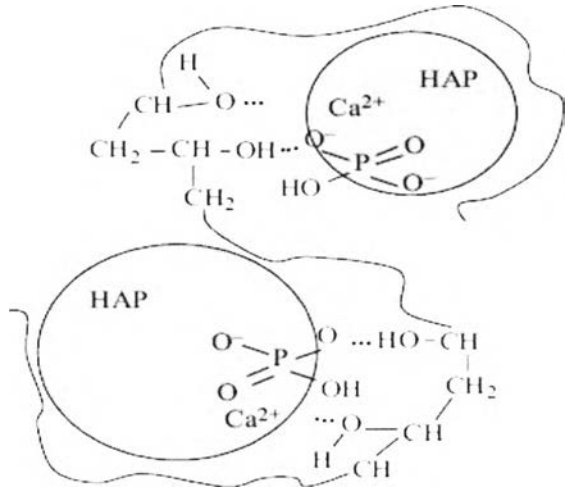

Figure 4.10 Diagram illustrating the interaction of HAp and PVA. (Safronova *et al.*, 2007)

Density, also an important physical property of the aerogel material, was determined by dividing the aerogel weight after removing water by the measured volume (eq. 8). (Krokida *et al.*, 1998)

$$\text{Density} = \frac{\text{Weight of aerogel material}}{\text{Volume of aerogel}} \qquad (8)$$

The densities of CaO/HAp - PVA hybrid aerogel using different percentages of PVA in water are shown in Fig. 4.11. The density of the aerogel material increased with increasing the PVA content in water or decreasing the water amount in the system. In our previous work (Lorjai *et al.*, 2009), water provides voids or pores in the aerogel material, thus, the decrease of water results in the decrease of pores, making the increase in the density. As for different types of calcium compound, the density of PVA-CaO aerogel was higher than that of PVA-HAp aerogel due to the higher volume shrinkage of PVA-CaO than that of PVA-HAp. (Safronova *et al.*, 2007)

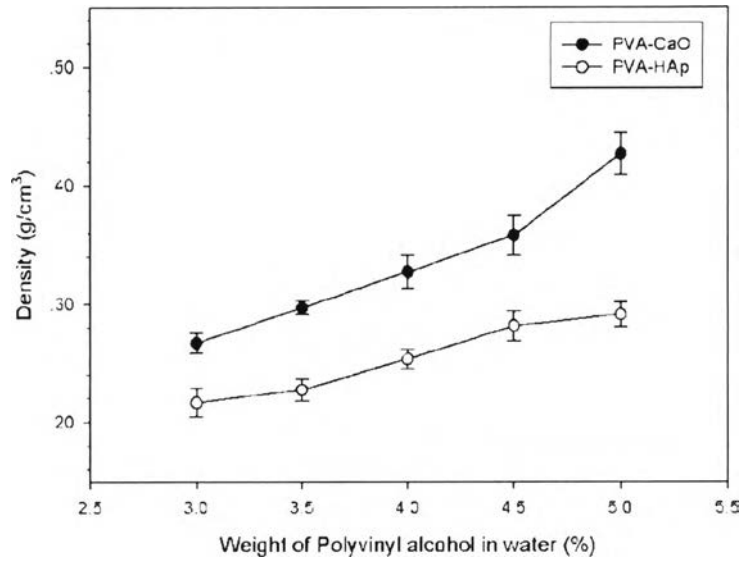

Figure 4.11 Density of CaO/HAp - PVA hybrid aerogel using different percentages of PVA in water.

Porosity of the aerogel material was characterized using helium pycnometry. This method provides skeletal volume and density of the determined material. The porosity is calculated using either equation 10 or 11. (Parmentier *et al.*, 2001)

$$\text{Porosity} = \frac{\text{Bulk Volume - Skeletal Volume}}{\text{Bulk Volume}} \times 100 \qquad (10)$$

$$\text{Porosity} = \left[1-\left(\frac{\text{Bulk Density}}{\text{Skeletal density}}\right)\right] \times 100 \qquad (11)$$

The porosities of PVA-CaO and PVA-HAp aerogel material decrease as the PVA content increase because the increasing PVA content in the solution affects to a decrease in the content of the void and the pore, as shown in Fig. 4.13 and 4.14, respectively, illustrating the morphologies of the porosities of PVA-CaO and PVA-HAp. (Agda *et al.*, 2009) However, the result of 3%PVA-CaO has lower porosity than 3.5% PVA-CaO probably due to aggregation of CaO in 3%PVA-CaO, as confirmed by the SEM micrograph in Fig. 4.13(a). Comparing between CaO and

HAp for a fixed PVA content, PVA-CaO had lower porosity because of lower compatibility and dispersion. From SEM micrographs at the same magnification (1k), it was found that the pore size of PVA-CaO was smaller than PVA-HAp because of the effect of the volume shrinkage.

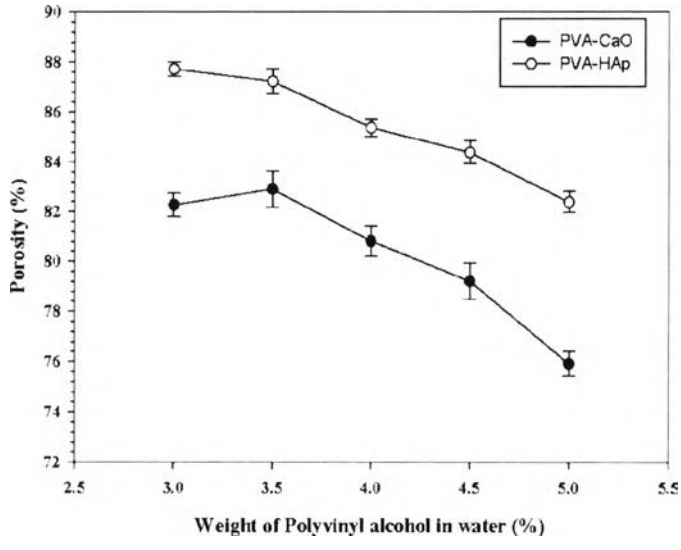

Figure 4.12 Porosity of CaO/HAp - PVA hybrid aerogel using different percentages of PVA in water.

Figure 4.15 shows the compressive strength of CaO/HAp-PVA hybrid aerogels using different percentages (3.0 to 5.0 %wt) of PVA in water, enhancing the compressive strength from 0.7508 to 2.9177 MPa for PVA-CaO and from 0.3809 to 1.3645 MPa for PVA-HAp. Another word, the increasing PVA content resulted in the increasing compressive strength due to the increases of the cell wall strength and the density of the materials, in which both factors generally influence on the fracture area for absorbing load and resistance to deformation. (Zhao *et al.*, 2011). Highly porous material has low cell wall strength and low density, related to low resistance to deformation. (Nie *et al.*, 2011 and Tavangarian *et al.*, 2011). Comparing between CaO and Hap, PVA-HAp had lower compressive strength than PVA-CaO at the same PVA content because PVA-HAp has lower density and bigger pore size.

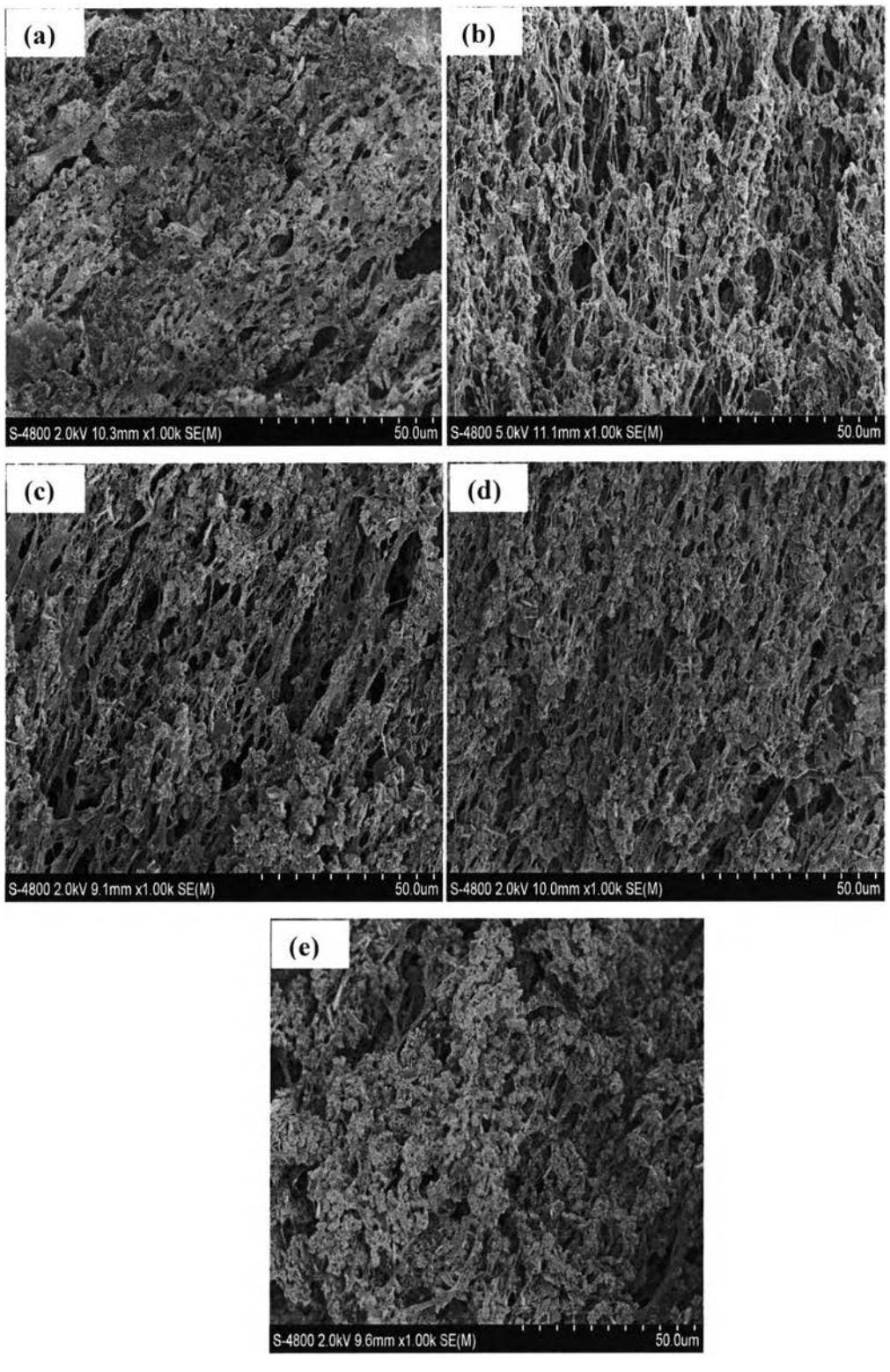

Figure 4.13 SEM micrographs of (a) 3%PVA-CaO, (b) 3.5%PVA-CaO, (c) 4%PVA-CaO (d) 4.5%PVA-CaO, and (e) 5% PVA-CaO.

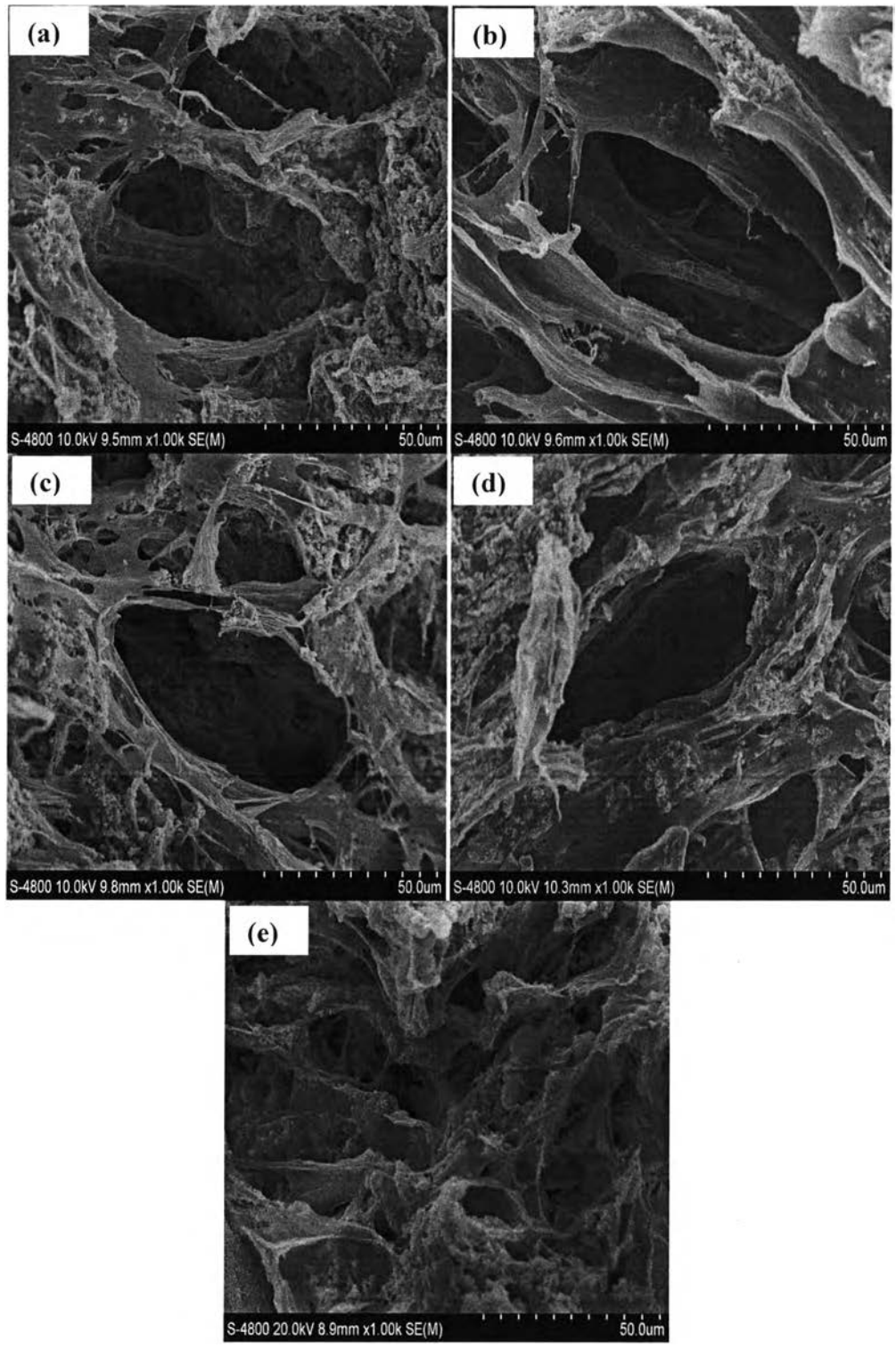

Figure 4.14 SEM micrographs of (a) 3%PVA-HAp, (b) 3.5%PVA-HAp, (c) 4%PVA-HAp (d) 4.5%PVA-Hap, and (e) 5% PVA-HAp.

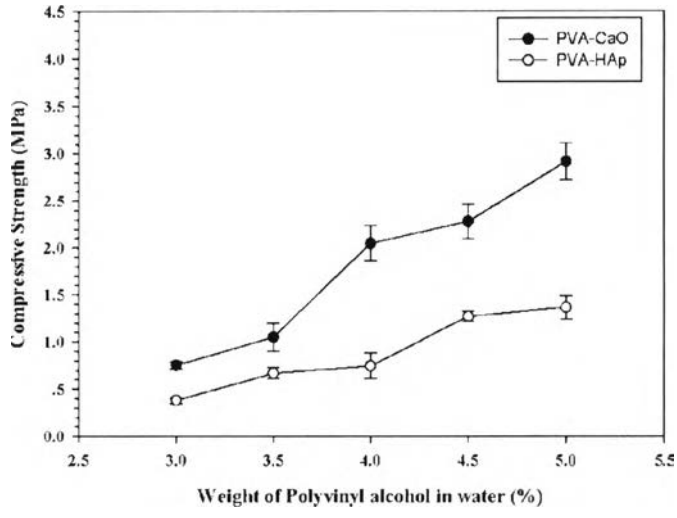

Figure 4.15 Compressive Strength of CaO/HAp – PVA hybrid aerogel using different percentages of PVA in water.

FT-IR spectra of the PVA-CaO and PVA-HAp hybrid aerogels are shown in Fig 4.16, containing all the characteristic peaks of PVA at 3400 (–OH stretching), 2930, 2900, and 1415 (asymmetric stretching, symmetric stretching and wagging of CH_2, respectively), and 1143 cm^{-1} (C-O stretching). However, there is one peak indicating type of calcium compound, see Fig.4.16 (a). Two important peaks of PVA-CaO at 1450 and 3640 cm^{-1} attributed to C-O stretching of the carbonate group of calcium carbonate residue and -OH group of calcium hydroxide containing in calcium oxide, respectively. Figure 4.16 (b) shows important characteristic peaks of PO_4^{3-}, indicating the hydroxyapatite at peak 1050, 1020, 961, 572, and 470 cm^{-1}. (Nie *et al.*, 2011 and Sanosh *et al.*, 2009)

Figure 4.17 shows TGA thermograms of the PVA-CaO/HAp hybrid aerogel materials. TGA thermogram of PVA-CaO had three-step-degradation. According to Peng *et al.* (2007), the first degradation step at 200°–350 °C is the elimination reaction of the polyvinyl alcohol with 10 %weight loss to give polyenes and water product, as shown in the Fig 4.18a. However, the degradation temperature in the first step is not high enough to break the backbone chain of polyenes.

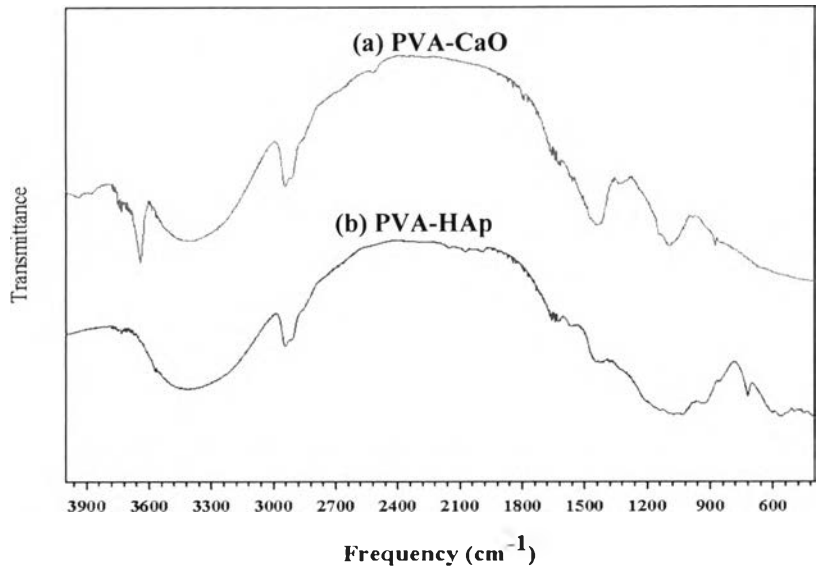

Figure 4.16 FT-IR spectra of (a) PVA-CaO and (b) PVA-HAp hybrid aerogels.

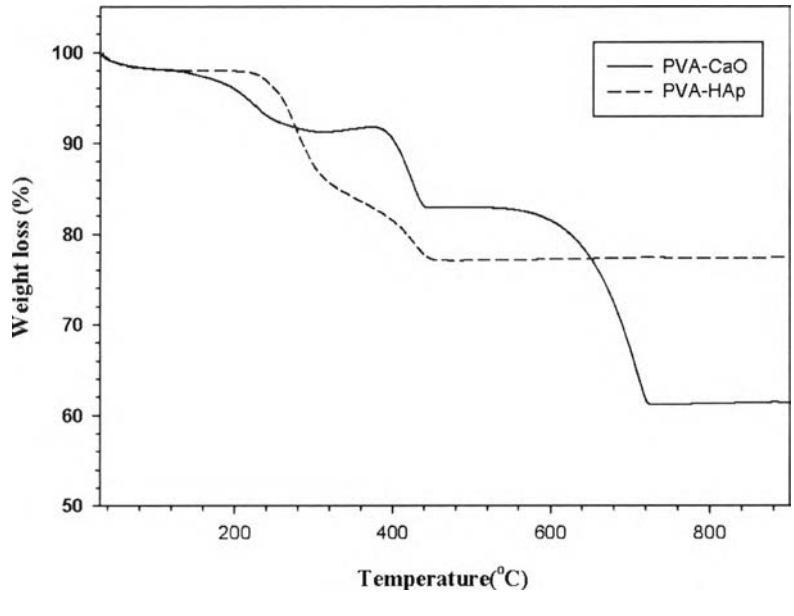

Figure 4.17 TGA thermograms of of CaO/HAp – PVA hybrid aerogels.

The second degradation step at 350°–450 °C is chain-scission reaction of polyenes with 10 %weight loss, as shown in the Fig 4.18b, to low-molecular-weight

polyenes and gaseous product. The last transition region at 600°–700 °C is the transformation of calcium carbonate residue to calcium oxide with the weight loss of about 18%, as shown equation 1 (Engin *et al.*, 2006). TGA thermogram of PVA-HAp provided two-step-degradation, corresponding to the elimination reaction of the polyvinyl alcohol and chain-scission reaction of polyenes with 10, and 10% weight loss, respectively. From the experiment, the suitable ratio of PVA and CaO/Hap to result in the similar TGA thermogram to the results studied by Yang *et al.* in 2008 is 80:20.

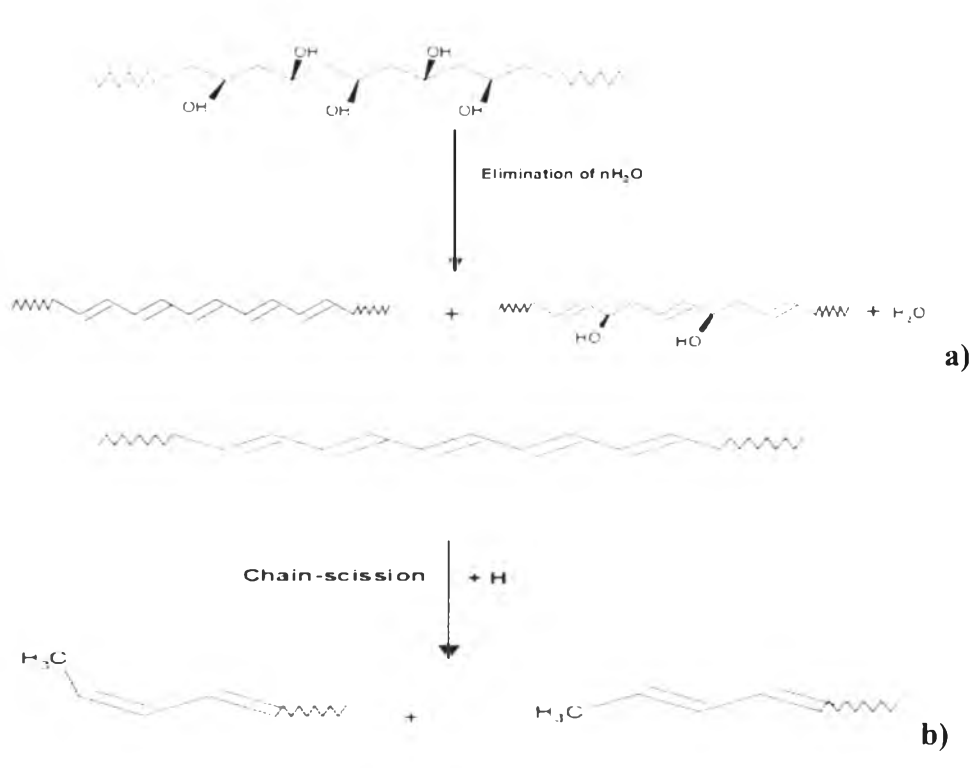

Figure 4.18 Diagram of (a) Elimination reaction of water and (b) Chain-scission reactions of polyenes. (Peng *et al.*, 2007)

The surface areas of the synthesized aerogels were calculated from Brunauer-Emmett-Teller (BET), as summarized in Table 4.1. The effect of the weight percentage of PVA in water of the PVA-CaO aerogel was found that the increasing PVA content led to a decrease of the surface area because the increasing